Resonance Raman Spectroscopic Study of Phenoxyl Radical Complexes

Robert Schnepf, Achim Sokolowski, Jochen Müller, Vinzenz Bachler, Karl Wieghardt,* and Peter Hildebrandt*

Contribution from the Max-Planck-Institut für Strahlenchemie, Stiftstrasse 34−36, D-45470 Mülheim, Germany

Received July 8, 1997

Abstract: Resonance Raman (RR) spectroscopy has been employed to study *coordinated* phenoxyl radicals (M = Ga, Sc, Fe) which were electrochemically generated in solution by using 1,4,7-triazacyclononane-based ligands containing one, two, or three *p*-methoxy or *p*-*tert*-butyl N-substituted phenolates, i.e., 1,4,7-tris(3,5-di-*tert*-butyl-2-hydroxybenzyl)-1,4,7-triazacyclononane ($^3L^{but}$), 1,4,7-tris(3-*tert*-butyl-5-methoxy-2-hydroxybenzyl)-1,4,7-triazacyclononane ($^3L^{met}$), 1,4-bis(3-*tert*-butyl-5-methoxy-2-hydroxybenzyl)-7-ethyl-1,4,7-triazacyclononane ($^2L^{met}$), and 1-(3-*tert*-butyl-5-methoxy-2-hydroxybenzyl)-4,7-dimethyl-1,4,7-triazacyclononane ($^1L^{met}$). A selective enhancement of the vibrational modes of the phenoxyl chromophores is achieved upon excitation in resonance with the $\pi \rightarrow \pi^*$ transition at ca. 410 nm. The interpretation of the spectra was supported by quantum chemical (density functional theory) calculations which facilitate the vibrational assignment for the coordinated phenoxyl radicals and provide the framework for correlations between the RR spectra and the structural and electronic properties of the radicals. For the uncoordinated phenoxyl radicals the geometry optimization yields a semiquinone character which increases from the unsubstituted to the *p*-methyl- and the *p*-methoxy-substituted radical. This tendency is indicated by a steady upshift of the ν_{8a} mode which predominantly contains the $C_{ortho}-C_{meta}$ stretching coordinate, thereby reflecting strengthening of this bond. The calculated normal-mode frequencies for these radicals are in a good agreement with the experimental data constituting a sound foundation for extending the vibrational analysis to the 2,6-di-*tert*-butyl-4-methoxyphenoxyl which is the building block of the macrocyclic ligands $^3L^{met}$, $^2L^{met}$, and $^1L^{met}$. The metal-coordinated radical complexes reveal a similar band pattern as the free radicals with the modes ν_{8a} and ν_{7a} (C═O stretching) dominating the RR spectra. These two modes are sensitive spectral indicators for the structural and electronic properties of the coordinated phenoxyl radicals. A systematic investigation of complexes containing different ligands and metal ions reveals that two parameters control the semiquinone character of the phenoxyls: (i) an electron-donating substituent in the *para* position which can accept spin density from the ring and (ii) an electron-accepting metal ion capable of withdrawing excess electron density, introduced by additional electron-donating substituents in *ortho* positions. It appears that both effects, which are reflected by (i) the frequency of the mode ν_{8a} and (ii) the frequency difference of the modes ν_{8a} and ν_{7a}, balance an optimum electron density distribution in the phenoxyl radical. Along similar lines, it has been possible to interpret the RR spectral changes between the Fe monoradical, $[Fe(^3L^{met})]^{+\bullet}$, and diradical, $[Fe(^3L^{met})]^{2+\bullet\bullet}$, complexes. Both the parent as well as the radical complexes of Fe exhibit a phenolate-to-iron charge transfer band >500 nm. Excitation in resonance with this transition yields a selective enhancement of the vibrational modes of the coordinated phenolates which reveal a significantly more complex band pattern than the coordinated phenoxyls. For a large number of phenolate modes, distinct differences in frequencies and relative intensities were found between the parent and the monoradical Fe complexes implying that oxidation of one phenolate affects the structures and electron density distributions in the ground and excited states of the remaining phenolates. These results are discussed in relation to the structure of the copper-coordinated tyrosyl radical in the active site of galactose oxidase.

Introduction

In a number of redox enzymes such as ribonucleotide reductase, cytochrome *c* peroxidase, prostaglandin synthase, or the oxygen evolving complex of photosystem II, radicals of aromatic amino acids (i.e., tryptophan and tyrosine) are known to play a crucial role during the catalytic reaction cycle.[1−4] A particularly intriguing example is galactose oxidase (GO), which catalyzes the oxidation of a variety of alcohols.[5] Its active site contains a (substituted) tyrosyl radical coordinated to a copper(II), constituting a novel mononuclear center in which both the

* To whom correspondence should be addressed.

(1) (a) Sjöberg, B.-M.; Larson, A. *EMBO J.* **1986**, *5*, 2037−2040. (b) Bollinger, J. M., Jr.; Edmondson, D. E.; Huynh, B. H.; Filley, J.; Norton, J. R.; Stubbe, J. *Science* **1991**, *253*, 292−298.

(2) (a) Yonetani, T. *J. Biol. Chem.* **1965**, *240*, 4509−4514. (b) Huyett, J. E.; Doan, P. E.; Gurbiel, R.; Houseman, A. L. P.; Sivaraja, M.; Goodin, D. B.; Hoffman, B. M. *J. Am. Chem. Soc.* **1995**, *117*, 9033−9041.

(3) (a) Karthein, R.; Dietz, R.; Nastainczyk, W.; Ruf, H. H. *Eur. J. Biochem.* **1988**, *171*, 313−320. (b) Smith, W. L.; Eling, T. E.; Kulmacz, R. J.; Marnett, L. J.; Tsai, A. *Biochemistry* **1992**, *31*, 3−7.

(4) (a) Barry, B. A.; El-Deeb, M. K.; Sandusky, P. O.; Babcock, G. T. *J. Biol. Chem.* **1990**, *265*, 20139−20143. (b) Hoganson, C. W.; Babcock, G. T. *Biochemistry* **1992**, *31*, 11874−11880.

S0002-7863(97)02269-5 CCC: $15.00
Published on Web 02/28/1998

metal ion and a ligand are redox-active. Recently, evidence was provided for the same type of active site in glyoxal oxidase[6] indicating that a metal(copper)-coordinated tyrosyl radical is not a unique redox center of a specific enzyme but may represent a common structural motif for a novel group of enzymes.

More insight into the structural details of the active site has been achieved by the crystal structure of the inactive form of GO in which the tyrosyl ligand is reduced to a tyrosinate.[7] This ligand as well as a second tyrosinate, two histidines, and an exogenous buffer-derived acetate ligand (pH 4.5), which at pH 7.0 is replaced by a water molecule, have been shown to provide a square-pyramidal coordination sphere at the copper center. Whereas these data reveal the geometry of the active site and its environment in the inactive form of the enzyme, there are still numerous questions concerning the mechanism of the electron-transfer processes as well as the structural parameters which control the stability and reactivity of the radical ligand in the active form.

Spectroscopic techniques such as electron paramagnetic resonance (EPR) or resonance Raman (RR) spectroscopy can be employed advantageously to elucidate structure−function relationships of these enzymes.[8,9] However, the extraction of structural information from the spectra is still a considerable challenge, particularly since the chemistry and spectroscopy of metal-coordinated radicals are far from being fully understood.

Our approach to narrow this gap is based on model compounds which are designed to mimic the structural, chemical, and physical properties of the enzymatic active sites. In previous studies,[10−14] we have demonstrated that (transition) metal complexes containing ligands of the type 1,4,7-tris(*o*-hydroxybenzyl)-1,4,7-triazacyclononane in its trisanionic form (Figure 1) fulfill these requirements inasmuch as their electrochemical oxidation yields in some instances ligand-centered phenoxyl radicals. These oxidation products are relatively stable, and in one case, even a crystal structure was obtained.[11] The spectroscopic data for these radical complexes obtained so far reveal striking similarities in the electronic and magnetic properties as compared to the active sites of the target enzymes.[5,15,16] Thus, a more systematic investigation of such complexes which is the objective of the present study holds promise to contribute to a better understanding of structural and mechanistic aspects which are of relevance for the biocatalytic processes.

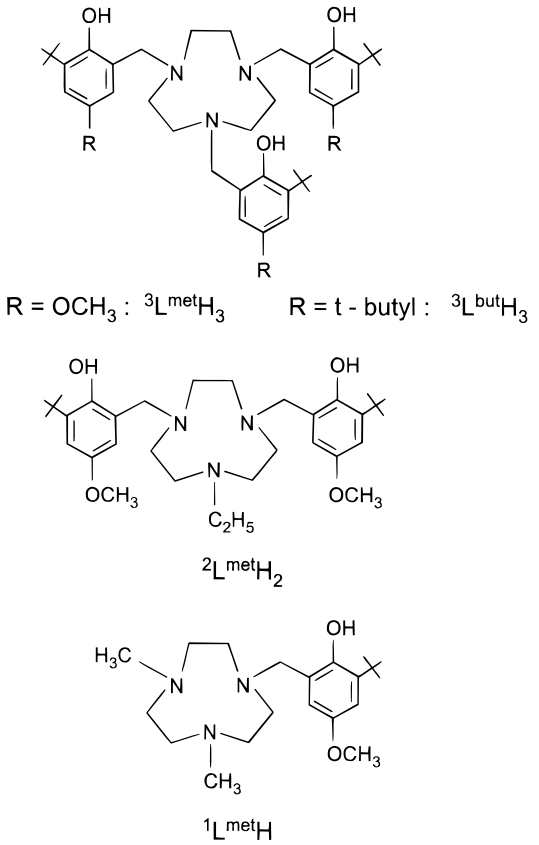

Figure 1. Structural formulas of the macrocyclic phenolate ligands.

In this work we have employed RR spectroscopy which can selectively probe the vibrational spectra of the coordinated aromatic ligands upon excitation in resonance with the ligand-centered electronic transitions.[12−14,16,17] As a starting point, we have focused on the vibrational analysis of free phenoxyl radicals, carrying different substituents, to model as closely as possible the substituted phenoxyl arms of the macrocyclic ligand (Figure 1). Subsequently, we have extended the assignment to the phenoxyl radicals coordinated to different metal ions. The RR spectra of various metal radical complexes were analyzed with special emphasis on the metal-sensitive RR bands *in an attempt to extract spectral markers for structural and electronic properties of these complexes*. To assess the effect of the additional coordinating groups in the octahedral complexes we have modified the macrocyclic ligands of iron complexes. These complexes also provide the possibility to probe either the phenoxyl or the phenolate ligands, thereby allowing us to study the effect of radical formation on the remaining phenolates and, thus, on the electron density distribution in the entire metal complex.

Experimental Section

Synthesis. The syntheses of the tris(phenolato) complexes of Sc^{III}, Ga^{III}, and Fe^{III} were published elsewhere.[10] The preparations of the ligands $^3L^{met}H_3$, $^3L^{but}H_3$, and $^1L^{met}H_1$ have been described previously.[10,14] The synthesis of $^2L^{met}H_2$ is similar and will be discussed in detail elsewhere.

[Fe($^2L^{met}$)Cl]. To a solution of $^2L^{met}H_2$ (0.54 g; 1.0 mmol) in methanol (30 mL) was added $FeCl_2$ (0.13 g; 1.0 mmol). After a few

(5) (a) Babcock, G. T.; El-Deeb, M. K.; Sandusky, P. O.; Whittaker, M. M.; Whittaker, J. W. *J. Am. Chem. Soc.* **1992**, *114*, 3727−3734. (b) Whittaker, M. M.; Chuang, Y.-Y.; Whittaker, J. W. *J. Am. Chem. Soc.* **1993**, *115*, 10029−10035.

(6) Whittaker, M. M.; Kersten, P. J.; Nakamura, N.; Sanders-Loehr, J.; Schweizer, E. S.; Whittaker, J. W. *J. Biol. Chem.* **1996**, *271*, 681−687.

(7) Ito, N.; Phillipps, S. E. V.; Stevens, C.; Orgel, Z. B.; McPherson, M. J.; Keen, J. N.; Yadav, K. D. S.; Knowles, P. F. *Nature* **1991**, *350*, 87−90.

(8) Spiro, T. G., Ed. *Biological Applications of Raman Spectroscopy*; Wiley: New York, 1988; Vol. III.

(9) Pilbrow, J. R.; Hanson, G. R. *Methods Enzymol.* **1993**, *227*, 330−353.

(10) Adam, B.; Bill, E.; Bothe, E.; Goerdt, B.; Haselhorst, G.; Hildenbrand, K.; Sokolowski, A.; Steenken, S.; Weyhermüller, T.; Wieghardt, K. *Chem. Eur. J.* **1997**, *3*, 308−319.

(11) Sokolowski, A.; Bothe, E.; Bill, E.; Weyhermüller, T.; Wieghardt, K. *Chem. Commun.* **1996**, 1991−1972.

(12) Sokolowski, A.; Leutbecher, H.; Weyhermüller, T.; Schnepf, R.; Bothe, E.; Bill, E.; Hildebrandt, P.; Wieghardt, K. *J. Biol. Inorg. Chem.* **1997**, *2*, 444−453.

(13) Sokolowski, A.; Adam, B.; Weyhermüller, T.; Kikuchi, A.; Hildenbrand, K.; Schnepf, R.; Hildebrandt, P.; Bill, E.; Wieghardt, K. *Inorg. Chem.* **1997**, *36*, 3702−3710.

(14) Sokolowski, A.; Müller, J.; Weyhermüller, T.; Schnepf, R.; Hildebrandt, P.; Hildenbrand, K.; Bothe, E.; Wieghardt, K. *J. Am. Chem. Soc.* **1997**, *119*, 8889−8900.

(15) Whittaker, M. M.; DeVito, V. L.; Asher, S. A.; Whittaker, J. W. *J. Biol. Chem.* **1989**, *264*, 7104−7106.

(16) McGlashen, M. L.; Eads, D. D.; Spiro, T. G.; Whittaker, J. W. *J. Phys. Chem.* **1995**, *99*, 4918−4922.

(17) Que, L., Jr. In *Biological Applications of Raman Spectroscopy*; Spiro, T. G., Ed.; Wiley: New York, 1988; Vol. III, pp 491−521.

minutes of stirring at room temperature in the presence of air, a dark blue solution was obtained. Within a few hours, a microcrystalline blue precipitate formed, which was collected by filtration and recrystallized from methanol (yield: 0.3 g; 48%). Anal. Calcd for $C_{32}H_{49}N_3O_4ClFe$: C, 60.9; H, 7.8; N, 6.7. Found: C, 61.0; H, 7.8; N, 6.8. FAB-MS (MNBA): *m*/*z* (rel intens, %) 630 {Fe($^2L^{met}$)Cl]$^+$, 10}, 595 {[Fe($^2L^{met}$)]$^+$, 100}.

[Fe($^1L^{met}$)Cl$_2$]. A blue microcrystalline precipitate of [Fe($^1L^{met}$)Cl$_2$] was obtained by following the procedure given above for [Fe($^2L^{met}$)Cl] by using $^1L^{met}$ as the ligand (0.2 g; 46%). Anal. Calcd for $C_{20}H_{34}N_3O_2Cl_2Fe$: C, 50.5; H, 7.2; N, 8.8. Found: C, 50.6; H, 7.3; N, 8.7. FAB-MS (MNBA): *m*/*z* (rel intens, %) 474 {Fe($^1L^{met}$)Cl$_2$]$^+$, 10}, 439 {Fe($^1L^{met}$)Cl]$^+$, 100}, 404 {[Fe($^1L^{met}$)]$^+$, 65}.

Electrochemistry. Coulometric experiments were performed with EG&G equipment (potentiostat/galvanostat, model 273A). The electrochemistry of the metal complexes has been investigated by cyclic and square-wave voltammetry in CH_3CN solution containing 0.1 M [N(*n*-but)$_4$]PF$_6$ as supporting electrolyte. The radical complexes were generated by controlled-potential coulometry in CH_3CN solution containing 0.1 M [N(*n*-but)$_4$]PF$_6$. The uncoordinated radical, [P^{met}]$^\bullet$, was generated by a two-phase oxidation from the corresponding phenol in CCl_4 with an aqueous solution of $[Fe(CN)_6]^{3-}$. In the cyclic voltammogram of [Fe($^2L^{met}$)Cl], two reversible one-electron-transfer waves at redox potentials of 0.21 and 0.51 V vs the ferrocenium/ferrocene (Fc^+/Fc) couple were found, whereas, for [Fe($^1L^{met}$)Cl$_2$], one reversible one-electron-transfer wave at $E_{1/2} = 0.35$ V was observed. The redox potentials of the other complexes have been published previously.[10−14]

UV−Vis Absorption Spectroscopy. Electronic absorption spectra of CH_3CN solutions of complexes were recorded on a Perkin-Elmer Lambda 19 spectrometer (range: 190−1300 nm) at ambient temperature. Spectra of the electrochemically generated radical complexes were recorded in CH_3CN containing 0.10 M [N(*n*-but)$_4$]PF$_6$.

Resonance Raman Spectroscopy. RR spectra were recorded with a U1000 spectrograph (2400/mm holographic gratings) equipped with a liquid-nitrogen-cooled CCD detector (Instruments SA). The output of a dye laser (Coherent 899-01) and an argon ion laser (Coherent Innova 400) served as excitation sources. The laser power at the sample was about 50 mW. In order avoid photoinduced degradation, the sample which exhibits an optical density of ca. 1.5 at the excitation wavelength was deposited in a rotating cell. The Raman scattered light was detected in 90° with a scrambler placed in front of the entrance slit of the spectrometer to account for the polarization sensitivity of the gratings. The spectral slit width was 2.8 cm^{-1}. The spectra, measured with an acquisition time of 15 s, were linearized in wavenumbers yielding an increment between 0.1 and 0.25 cm^{-1} and a total spectral range of ca. 100−250 cm^{-1}. Thus, several spectra covering different but overlapping ranges are combined to give the overview spectra displayed in this work. In these spectra, the contributions of the solvent and the supporting electrolyte are subtracted. The band-fitting analysis of these spectra was carried out according to Döpner et al.[18]

Quantum Chemical Calculations. All quantum chemical computations were performed by means of the Gaussian92/DFT suite of *ab initio* programs working under OpenVMS and were carried out on a DEC station 2000.[19] For density functional theory (DFT) computations we employed the Becke3LYP (B3LYP) combination of hybrid exchange and correlation functionals.[20] We used the FineGrid option for the numerical integrations required in the DFT procedure. For all neutral phenoxyl radicals, the 6-31G* basis sets were applied.[21] They are of double-ζ type for the valence electrons and augmented by d-polarization functions for the carbon and oxygen atoms. These basis sets used in B3LYP DFT computations produce vibrational frequencies which are close to experimental values.[22] An even closer agreement can be achieved by means of an appropriate scaling procedure.[22] In a previous study,[22b] the force fields, calculated for various organic compounds by DFT(B3LYP) and 6-31G* basis sets, were scaled by a global set of 10 scaling factors. This scaling yielded an overall root mean standard deviation of the calculated frequencies from the experimental data of less than 11 cm^{-1}. In this work, we have used the root of the mean value of these factors, i.e., 0.9744, to scale just the frequencies. We have found that this simplified scaling procedure provides a sufficient accuracy for a safe assignment.

The phenoxyl radicals are open-shell molecules with a doublet ground state. We computed them by means of the unrestricted Hartree−Fock (UHF) method.[23] The UHF wave functions are not eigenfunctions of the total spin operator S^{**2}.[24] Thus, the computed UHF wave functions for the phenoxyl radicals do not describe a pure doublet state. However, spin contaminations of higher spin multiplicities, in particular quartet components, are small. This was indicated by the expectation values over S^{**2} which are close to 0.75.

In the phenolate anion, the negative charge results from an additional electron, only weakly bound to the molecular skeleton. The proper theoretical treatment of weakly bound extra electrons in anions has been studied carefully in the past.[25] One of the essential requirements is the employment of basis sets with diffuse functions. They allow the extra electron to become bonded at the periphery of the molecule. To simulate such a bonding, we applied for the phenolate the 9s5p/4s2p basis set augmented with polarization functions. Moreover, for oxygen and carbon additional diffuse s and p functions are provided with exponents of 0.059 and 0.034, respectively.[26]

Results and Discussion

Quantum Chemical Calculations. Previous studies[11−13,27] have shown that the RR spectra of metal-coordinated phenoxyl radical complexes are dominated by bands which can readily be related to those of free phenoxyl radicals.[28−34] Hence, a reliable vibrational analysis of such radicals appears to be a prerequisite for extracting structural information from the RR spectra of the metal-coordinated complexes which are in the focus of the present study. While vibrational analyses of the unsubstituted phenoxyl radical have been carried out with both empirical and quantum chemical force fields,[33−37] little is known about the effect of ring substituents on the geometry and the vibrational modes of the radicals.[33]

(18) Döpner, S.; Hildebrandt, P.; Mauk, A. G.; Lenk, H.; Stempfle, W. *Spectrochim. Acta* **1996**, *51A*, 573−584.

(19) Frisch, M. J.; Trucks, G. W.; Schlegel, H. B.; Gill, P. M.; Johnson, B. G.; Wong, M. W.; Foresman, J. B.; Robb, M. A.; Head-Gordon, M.; Replogle, E. S.; Gouperts, R.; Andres, J. L.; Raghavadari, K.; Binkley, J. S.; Gonzales, C.; Martin, R. L.; Fox, D. J.; Defrees, D. J.; Baker, J.; Stewart, J. J. P.; Pople, J. A. *Gaussian 92/DFT*, Revision G.4; Gaussian, Inc.: Pittsburgh, PA, 1993.

(20) (a) Becke, A. D. *J. Chem. Phys.* **1993**, *98*, 5648−5652. (b) Lee, G.; Young, W.; Parr, R. G. *Phys. Rev.* **1988**, *B37*, 785−789. (c) Miehlich, B.; Savin, A.; Stoll, H.; Preuss, H. *Chem. Phys. Lett.* **1989**, *157*, 200−206.

(21) (a) Hehre, W. J.; Ditchfield, R.; Pople, J. A. *J. Chem. Phys.* **1972**, *56*, 2257−2261. (b) Hariharan, P. C.; Pople, J. A. *Theor. Chim. Acta* **1973**, *28*, 213−222. (c) Gordon, M. S. *Chem. Phys. Lett.* **1980**, *76*, 163−168. (d) Clark, T.; Chandrasekhar, J.; Spitznagel, G. W.; Schleyer, P. v. R. *J. Comput. Chem.* **1983**, *4*, 294−301.

(22) (a) Rauhut, G.; Pulay, P. *J. Phys. Chem.* **1995**, *99*, 3093−3100. (b) Magdó, I.; Németh, K.; Hildebrandt, P.; Mark, F. Unpublished results.

(23) Pople, J. A.; Nesbet, R. K. *J. Chem. Phys.* **1954**, *22*, 571−572.

(24) Szabo, A.; Ostlund, N. S. *Modern Quantum Chemistry*; McGraw-Hill: New York, 1982; p 205.

(25) Kalcher, J.; Sax, A. F. *Chem. Rev.* **1994**, *94*, 2291−2318.

(26) Dunning, T. H.; Hay, P. J. *Modern Theoretical Chemistry*; Plenum: New York, 1976.

(27) (a) Zurita, D.; Gautier-Luneau, I.; Ménage, S.; Pierre, J. L.; Sain-Adam, E. *J. Biol. Inorg. Chem.* **1997**, *2*, 46−55. (b) Halfen, J. A.; Jazdzewski, B. A.; Mahapatra, S.; Berreau, L. M.; Wilkinson, E. C.; Que, L., Jr.; Tolman, W. B. *J. Am. Chem. Soc.*, **1997**, *119*, 8217−8227.

(28) Tripathi, G. N. R. In *Time-Resolved Spectroscopy*; Clark, R. J. H., Hester, R. E., Eds.; Wiley: New York, 1989; pp 157−218.

(29) Tripathi, G. N. R.; Schuler, R. H. *Chem. Phys. Lett.* **1983**, *98*, 594−596.

(30) Tripathi, G. N. R.; Schuler, R. H. *J. Phys. Chem.* **1988**, *92*, 5129−5133.

(31) Johnson, C. R.; Ludwig, M.; Asher, S. A. *J. Am. Chem. Soc.* **1986**, *108*, 905−912.

(32) Beck, S. M.; Brus, L. E. *J. Chem. Phys.* **1982**, *76*, 4700−4704.

(33) Qin, Y.; Wheeler, R. A. *J. Am. Chem. Soc.* **1995**, *117*, 6083−6092.

(34) Mukherjee, A.; McGlashen, M. L.; Spiro, T. G. *J. Phys. Chem.* **1995**, *99*, 4912−4917.

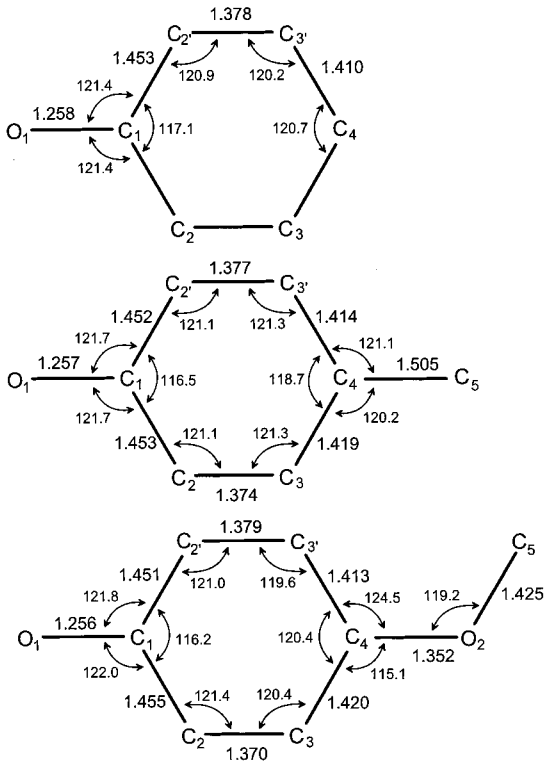

Figure 2. Calculated geometries (heavy atom frame) of the phenoxyl (top), *p*-methylphenoxyl (middle), and *p*-methoxyphenoxyl radicals (bottom). Bond angles are given in degrees and bond distances in angstroms.

We have employed DFT calculations using the three-parameter exchange-correlation functional B3LYP. This method has been demonstrated to provide reliable force fields for organic compounds including second-row elements (C, N, O, H)[22] and has, in fact, been successfully employed by Qin and Wheeler[36] for the analysis of the (unsubstituted) phenoxyl radical. We have extended these calculations to the *p*-methyl- and *p*-methoxy-substituted phenoxyl radicals which can be regarded as simple models for the building blocks of the L^{but} and L^{met} macrocyclic ligands shown in Figure 1.

Calculated Geometries. The geometry optimization yields planar ring structures of the unsubstituted phenoxyl as well as of the *para*-substituted methyl- and methoxyphenoxyl radicals. The geometrical parameters of the heavy-atom frame are displayed in Figure 2, and the bond distances are summarized in Table 1. The results for the unsubstituted phenoxyl radical (PhO•) which are identical to those obtained by Qin and Wheeler[36] reveal a substantial shortening of the C_2-C_3 bonds and an elongation of the C_1-C_2 and C_3-C_4 bonds as compared to aromatic ring systems.[38] Since, in addition, the C_1-O_1 bond length is also relatively shorter compared to that of the phenolates, these data indicate that the phenoxyl radical exhibits a semiquinone-like structure. Introducing a methyl and a methoxy group in the *para* position lowers the symmetry from C_{2v} to C_s. The substituents are oriented in such a way that only the plane of symmetry is preserved. Consequently, the C_2 and $C_{2'}$ (*ortho*) as well as the C_3 and $C_{3'}$ (*meta*) positions are no longer equivalent, which is in fact reflected in slight differences in the calculated bond distances (Table 1). The *para* substituents do not affect the geometry of the phenoxyl ring significantly. An increase of 0.007 Å is calculated for $C_{meta}-C_{para}$ bond distances in both *p*-methylphenoxyl (*p*-CH_3−PhO•) and *p*-methoxy phenoxyl (*p*-CH_3O−PhO•) which agrees very well with the results for the phenoxyl and tyrosyl radical by Qin and Wheeler[33] who have employed the DFT(SVWN) method. This agreement also holds for the even smaller changes of the $C_{ortho}-C_{meta}$ and O_1-C_1 bond distances which slightly decrease in the order PhO• > *p*-CH_3−PhO• (tyrosyl; see Qin and Wheeler[33]) > *p*-CH_3O−PhO• suggesting that this shortening is significant. This view is supported by experimental RR data discussed below. The bond length changes are accompanied by a small decrease of the $C_2C_1C_{2'}$ bond angle.

Table 1. Calculated Bond Distances (Å), Spin Densities, and Mulliken π-Overlap Populations of Phenoxyl Radicals[a]

	PhO•	*p*-CH_3−PhO•	*p*-CH_3O−PhO•
	Bond Distances		
C_1-O_1	1.258	1.257	1.256
C_1-C_{ortho}	1.453	1.452	1.453
$C_{ortho}-C_{meta}$	1.378	1.376	1.374
$C_{meta}-C_{para}$	1.410	1.417	1.417
$C_{para}-C_5$		1.505	
$C_{para}-O_2$			1.352
O_2-C_5			1.425
	Spin Densities		
O_1	0.444	0.428	0.406
C_1	−0.117	−0.106	−0.082
C_{ortho}	0.323	0.308	0.273
C_{meta}	−0.172	−0.163	−0.122
C_{para}	0.407	0.399	0.305
O_2			0.079
C_5		−0.030	−0.008
	Mulliken π-Overlap Population		
C_1-O_1	0.1280	0.1293	0.1290
$C_{ortho}-C_{meta}$	0.1581	0.1628	0.1688

[a] For the atom numbering, see Figure 2. The spin densities for C_{ortho} and C_{meta} as well as the bond distances C_1-C_{ortho}, $C_{ortho}-C_{meta}$, and $C_{meta}-C_{para}$ of *p*-CH_3−PhO• and *p*-CH_3O−PhO• given in the table are average values since the C_2 and C_2, as well as the C_3 and C_3, atoms are not equivalent in the *para*-substituted phenoxyl radicals (see Figure 2).

Concomitant with the slight $C_{ortho}-C_{meta}$ bond length shortening, the Mulliken π-overlap population increases, confirming the increased double-bond character of this bond in the *p*-methyl- and *p*-methoxy-substituted phenoxyls (Table 1). This tendency is not as clearly seen for the C_1-O_1 bond for which the π-orbital population increases from PhO• to *p*-CH_3−PhO• but not further in *p*-CH_3O−PhO•.

The structural changes are also paralleled by variations of the spin densities which for O_1, C_{ortho}, and C_{para} decrease in the *para*-substituted phenoxyl radicals, most pronounced in *p*-CH_3O−PhO•, where spin density is transferred to the oxygen atom of the methoxy substituent (Table 1). Decreasing spin density on the O_1 and C_{ortho} atoms implies an increasing π-bond character of the O_1-C_1 and $C_{ortho}-C_{meta}$ bonds which correlates with the decrease of the corresponding bond lengths (Table 1). As far as the *p*-alkyl-substituted phenoxyl is concerned, the DFT-(SVWN) study on PhO• and tyrosyl[33] and very recent DFT calculations[39] provide similar tendencies although the absolute values differ from those of the present work, which is due to the different exchange functionals and basis sets employed. For PhO•, the only experimental data refer to the spin density ratios C_{para}/C_{ortho} and C_{para}/C_{meta} (rather than to the absolute values)

(35) Chipman, D. M.; Liu, R.; Zhou, X.; Pulay, P. *J. Chem. Phys.* **1994**, *100*, 5023−5035.
(36) Qin, Y.; Wheeler, R. A. *J. Chem. Phys.* **1995**, *102*, 1689−1697.
(37) Gunion, R. F.; Gilles, M. K.; Polak, M. L.; Lineberger, W. C. *Int. J. Mass Spectrosc. Ion Proc.* **1992**, *117*, 601−620.
(38) Sutton, L. E., Ed. *Tables of Interatomic Distances and Configurations in Molecules and Ions*; Eyre and Spottiswoode: Margate, U.K., 1965.
(39) Himo, F.; Gräslund, A.; Eriksson, L. A. *Biophys. J.* **1997**, *72*, 1556−1567.

Table 2. Frequencies (cm^{-1}) of Selected Modes of Uncoordinated Phenoxyl Radicals and Metal-Coordinated Phenoxyl Radical Complexes[a]

					$[M(^3L^{met})]^{+\bullet}$			$[M(^3L^{met})]^{\bullet}$	$[M(^3L^{met})H]^{+\bullet}$	$[M(^3L^{met})H_2]^{2+\bullet}$		$[M(^3L^{but})]^{+\bullet}$
mode[b]	PhO$^{\bullet}$	*p*-CH_3−PhO$^{\bullet}$	*p*-CH_3O−PhO$^{\bullet}$	$[P^{met}]^{\bullet}$	Ga	Sc	Fe	Zn	Cu	Cu	Zn	Ga
ν_{8a} (A_1)	1557	1577	1607	1590	1623	1628	1623	1615	1614	1620	1620	1597
[C_2C_3 s]	*1562*	*1578*	*1595*									
ν_{7a} (A_1)	1505	1517	1518	1511	1507	1506	1502	1510	1497	1494	1504	1513
[C_1O_1 s]	*1460*	*1476*	*1489*									
ν_{19a} (A_1)	1398	1407	1406	1391	1374	1373	1371	1386		1375	1386	1387
[CC s/CH b]	*1397*	*1410*	*1409*									
[C_4O_2 s]				1294	1309	1316	1312	1301	1303	1305	1303	
			1303									
ν_1 (A_1)	801	817	822	811	812	817	817	806			806	829
[ring br]	*790*	*800*	*801*									
ν_{6a} (A_1)	528	462		526	529	530	527	527			530	529
[ring def]	*517*	*450*	*514*									

[a] Key: PhO$^{\bullet}$, phenoxyl; *p*-CH_3PhO$^{\bullet}$, *p*-methyl phenoxyl; *p*-CH_3OPhO$^{\bullet}$, *p*-methoxyphenoxyl; $[P^{met}]^{\bullet}$, 2,6-di-*tert*-butyl-4-methoxyphenoxyl. Experimental data for $[P^{met}]^{\bullet}$, $[M(^3L^{met})]^{+\bullet}$ (M = Ga, Sc, Fe), and $[Ga(^3L^{but})]^{+\bullet}$ were obtained in the present work; those for $[Zn(^3L^{met})]^{\bullet}$, $[Cu(^3L^{met})H]^{\bullet+}$, and $[M(^3L^{met})H_2]^{2+\bullet}$ (M = Cu, Zn) were taken from our previous studies.[12,14] For $[Sc(^3L^{but})]^{+\bullet}$, only the frequencies of the modes ν_{8a} (1601 cm^{-1}) and ν_{7a} (1514 cm^{-1}) could be determined. The experimental frequencies for PhO$^{\bullet}$, *p*-CH_3PhO$^{\bullet}$, and *p*-CH_3OPhO$^{\bullet}$ were taken from Mukherjee et al.[34] and Tripathi and Schuler.[30] The calculated frequencies, as obtained by DFT(B3LYP) and scaled by a factor of 0.9744, are given in italics. [b] Mode numbering refers to Wilson's notation as adapted by Mukherjee et al.[34] The main character of the modes (in brackets) is indicated by the abbreviations s (stretch), b (in-plane bending), ring br (ring breathing), and ring def (ring deformation). The symmetry of the modes (in parentheses) refers to the unsubstituted phenoxyl.

with values of ca. 1.5 and 5.4, respectively,[40] which are in qualitative agreement with the present results (1.3 and 2.4) but are better reproduced by the DFT(SVWN) method (1.3 and 5.3).[33] To our knowledge, experimental data on substituted phenoxyl radicals are only reported for tyrosyl in solution and in proteins.[4b,41,42] These spin densities vary substantially, indicating that the molecular environment may strongly affect the spin distribution within the radicals and, consequently, that a comparison with the calculated data is less meaningful.

We conclude that the semiquinone character of the radical structure slightly increases from the unsubstituted to the *p*-methyl- and *p*-methoxy-substituted phenoxyls. This tendency can readily be understood in terms of the electron-donating effect of the *para* substituents which increases from hydrogen to the methyl group and even more to the methoxy group (stronger mesomeric effect) so that the $C_{ortho}-C_{meta}$ double-bond character is stabilized. It is interesting to note that the recent crystal structure of the $[Cr^{III}(^3L^{met})]^{+\bullet}$ radical complex provides experimental proof for the semiquinone-like geometry inasmuch as the C_2-C_3 and C_1-O_1 bond lengths are considerably shortened as compared to those of the reduced (trisphenolato) complex.[11]

Normal-Mode Calculations. The C_{2v} symmetry of the phenoxyl radical leads to 21 in-plane modes (11 A_1, 10 B_2) and 9 out-of-plane modes (3 A_2 and 6 B_1). For the sake of comparability with previous studies, we employ the widely accepted benzene-derived mode numbering as adapted to the phenoxyl radical by Mukherjee et al.[34] This notation agrees with that used by Chipman et al.[35] except that the modes ν_{18b} and ν_{9b} and the modes ν_{18a} and ν_{12} are interchanged. For the *para*-substituted phenoxyl radicals, the geometry optimization leads to C_s symmetry with 26 and 28 in-plane modes (A′) and 13 and 14 out-of-plane modes (A″) for *p*-methyl- and *p*-methoxyphenoxyl, respectively. Taking into account that the C_{2v} symmetry species A_1 and B_2 transform to A′ under symmetry lowering to C_s and, correspondingly, A_2 and B_1 to A″, one may extend the mode correlations from the unsubstituted to the *para*-substituted phenoxyl radicals. However, this does not imply that the normal-mode compositions are similar in all cases.

Quantum chemical force field calculations are associated with systematic errors which originate from the harmonic approximation and insufficient consideration of electron correlation effects. Such systematic errors can effectively be compensated by scaling the force fields as demonstrated by Pulay and coworkers.[22a] Thus, it is particularly remarkable that the present unscaled DFT(B3LYP) force fields yield frequencies that are in a good agreement with the experimental data reported previously.[34] For the unsubstituted phenoxyl radical the root mean standard (rms) deviation is 30 cm^{-1}, which is higher by only 50% than for scaled force fields calculated by significantly more rigorous methods (CAS−SCF; 18.7 cm^{-1}).[36] Hence, one may expect that further improvement of the standard deviation can be achieved by scaling the force field by an appropriate set of scaling factors.[22a] Within the scope of the present work, however, it is sufficient to employ a single factor for scaling the calculated frequencies so that a reliable assignment for most of the observed bands is possible. This scaling factor was taken as the average of a recently determined set of global scaling factors for DFT(B3LYP) force fields.[22b]

For the unsubstituted phenoxyl radical PhO$^{\bullet}$ RR frequencies have been reported by various authors[28−34] and recently discussed critically by Chipman et al.[35] and Mukherjee et al.[34] Table 2 compares the frequencies of some of the modes calculated in this work and the experimental data measured and compiled by Mukherjee et al.[34] In general, there is a good agreement between the experimental and the calculated data with a rms deviation of 20.0 cm^{-1}, which compares very well with previous studies.[33,35] Thus, we conclude that the DFT(B3LYP) method provides reliable assignments for the vibrational modes of PhO$^{\bullet}$ so that it can be extended to substituted phenoxyl radicals with confidence.

The RR spectrum of the *p*-methylphenoxyl (*p*-CH_3−PhO$^{\bullet}$) radical has been reported by Tripathi and Schuler[30] along with a tentative assignment which, in most cases, is supported by the present calculated data. The overall agreement between the

(40) (a) Neta, P.; Fessenden, R. W. *J. Phys. Chem.* **1974**, *78*, 523−529. (b) Stone, T. J.; Waters, W. A. *J. Chem. Soc.* **1964**, 213−218.

(41) (a) Bender, C. J.; Sahlin, M.; Babcock, G. T.; Barry, B. A.; Chandrashekar, T. K.; Salowe, S. P.; Stubbe, J.; Lindström, B.; Petersson, L.; Ehrenberg, A.; Sjöberg, B.-M. *J. Am. Chem. Soc.* **1989**, *111*, 8076−8083. (b) Rigby, S. E. J.; Nugent, J. H. A.; O'Malley, P. J. *Biochemistry* **1994**, *33*, 1734−1742.

(42) Warncke, K.; Babcock, G. T.; McCracken, J. *J. Am. Chem. Soc.* **1994**, *116*, 7332−7340.

calculated and the experimental data is similar to the case for PhO• with a standard deviation of 19.2 cm^{-1}. The RR frequencies of *p*-CH_3−PhO• do not differ strongly from those of the tyrosyl radical[33] except for the ν_{8a} mode, which is observed at a distinctly lower frequency (1565 cm^{-1} vs 1577 cm^{-1} in *p*-CH_3−PhO•). On the basis of DFT calculations, Qin and Wheeler[33] have suggested vibrational assignments for the tyrosyl radical which are in line with the assignments for *p*-CH_3−PhO• proposed in the present work. Also the RR frequencies of *p*-methoxyphenoxyl (*p*-CH_3O−PhO•)[30] are well predicted by the DFT(B3LYP) calculations with a rms deviation of 19.1 cm^{-1}. Again, there are only minor discrepancies in the vibrational assignments. Complete listings of the calculated modes of all three phenoxyl radicals as well as a more detailed discussion of the assignments are given in the Supporting Information.

Considering these results, it is remarkable that nearly all the modes, for which a comparison with experimental data is possible, nicely reproduce the tendencies noted in the measured RR spectra such as the frequency increase of modes ν_{8a} and ν_1 in the order PhO• < *p*-CH_3−PhO• < *p*-CH_3O−PhO• (Table 2). Also the behavior of the ν_{19a} mode, which is nearly at the same position in both *para*-substituted phenoxyls but ca. 10 cm^{-1} lower in the PhO•, is reliably predicted. The only serious deviation from the experimental data in all phenoxyl radicals is associated with the ν_{7a} mode which is invariably calculated too low (25−45 cm^{-1}). In addition, a substantial frequency upshift from *p*-CH_3−PhO• to *p*-CH_3O−PhO• is predicted which, however, is not observed. The ν_{7a} mode exhibits predominantly C_1−O_1 stretching character. Most likely, the C−O stretching is particularly sensitive to the molecular environment of the phenoxyl (solvation effects), which is not accounted for by the quantum chemical calculations. This is experimentally corroborated by the fact that the ν_{7a} mode of PhO• is found at 1505 cm^{-1} in alkaline aqueous solutions (Table 2) but at 1518 cm^{-1} at neutral pH[32,34] and for the tyrosyl radical this mode was observed at 1510 cm^{-1} in aqueous solution[31] but at 1498 cm^{-1} in ribonucleotide reductase.[43]

Modes ν_{8a} and ν_{7a} are of special interest inasmuch as their potential energy distributions are dominated by the C_2−C_3 and C_1−O_1 stretching coordinates, respectively, which both are characteristic indicators for a semiquinoid structure of the radical. Thus, an upshift of the ν_{8a} (ν_{7a}) frequency should reflect an increased double-bond character of the C_2−C_3 (C_1−O_1) bond, which in turn is paralleled by a contraction of the bond length and also by a decrease of the spin density at the O_1 and C_{ortho} positions (Table 1). In this respect, the calculations provide a consistent picture, regardless of the systematic deviations of the ν_{7a} mode frequencies from the experimental data. As displayed in Figure 3, the ν_{8a} and ν_{7a} frequencies reveal inverse relationships with the corresponding bond distances and the spin densities.

Vibrational Assignment of the 2,6-Di-*tert*-butyl-4-methoxyphenoxyl Radical. As the present DFT(B3LYP) calculations can predict the vibrational spectra of (substituted) phenoxyl radicals in a satisfactory fashion, these results form a sound basis for the vibrational analysis of the more complex phenoxyl derivative, i.e., 2,6-di-*tert*-butyl-4-methoxyphenoxyl ([P^{met}]•), which itself was not treated by quantum chemical methods. This compound, however, constitutes a building block for the macrocyclic ligands in the coordinated radical complexes (Figure 1). Sections of the RR spectra of [P^{met}]• which are excited at 413 nm in resonance with the $\pi \rightarrow \pi^*$ transition are displayed in Figure 4, and some of the frequencies as determined by a band-fitting analysis are included in Table 2. Note that the strongest band in the high-frequency region at 1511 cm^{-1} (Figure 4, top) is more intense by a factor of 3 than the strongest band in the low-frequency region at 526 cm^{-1} (Figure 4, bottom).

For the assignment of the observed bands, it is useful to keep in mind that excitation in resonance with a strong (allowed)

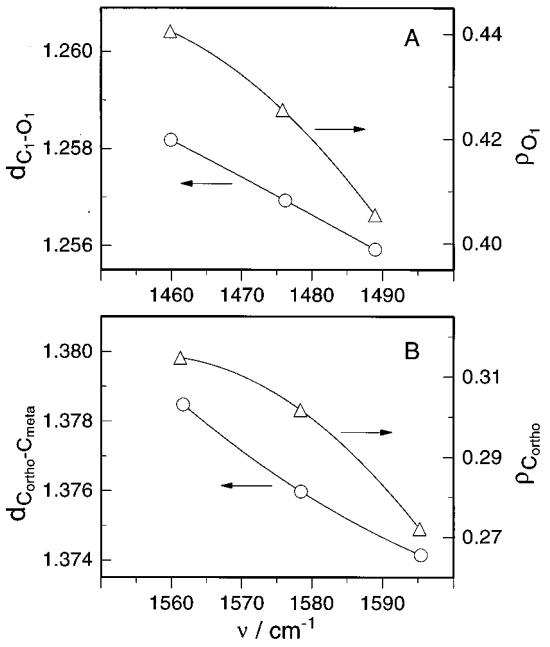

Figure 3. Correlations between bond distances (*d*; circles) and spin densities (*ρ*; triangles) and the frequencies of the modes ν_{7a} (A) and ν_{8a} modes (B) calculated for PhO•, *p*-CH_3−PhO•, and *p*-CH_3O−PhO•.

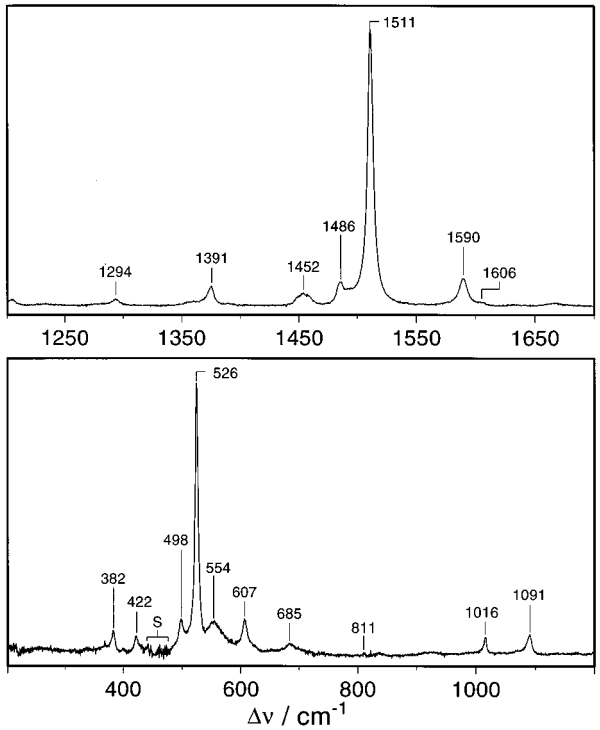

Figure 4. RR spectrum of 2,6-di-*tert*-butyl-4-methoxyphenoxyl radical excited at 413 nm in the high- (top) and low-frequency regions (bottom). The Raman bands of the solvent (CCl_4) are subtracted. Subtraction artifacts are denoted by "S".

(43) Backes, G.; Sahlin, M.; Sjöberg, B.-M.; Loehr, T. M.; Sanders-Loehr, T. *Biochemistry* **1989**, *28*, 1923−1929.

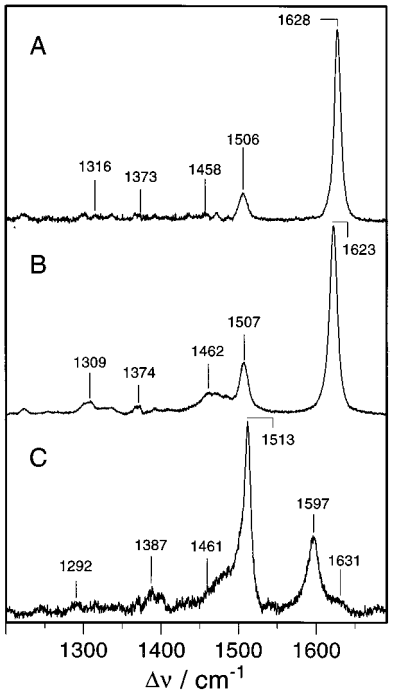

Figure 5. RR spectra of $[Sc(^3L^{met})]^{+\bullet}$ ($\lambda_{exc} = 432$ nm; A), $[Ga(^3L^{met})]^{+\bullet}$ ($\lambda_{exc} = 425$ nm; B), and $[Ga(^3L^{but})]^{+\bullet}$ ($\lambda_{exc} = 418$ nm; C) in the high-frequency region. The Raman bands of the solvent ($CH_3CN/LiClO_4$) are subtracted.

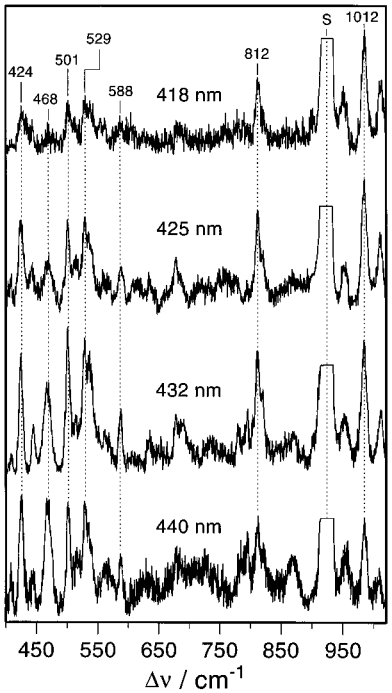

Figure 6. RR spectra of $[Ga(^3L^{met})]^{+\bullet}$ in the low-frequency region excited at different wavelengths. The strongest Raman band of the solvent ($CH_3CN/LiClO_4$), denoted by "S", could not be subtracted completely without causing subtraction artifacts.

electronic transition provides RR intensity for the totally symmetric modes. For the phenoxyl radical (C_{2v}) and the *para*-substituted phenoxyl radicals (C_s), these are the A_1 and A′ modes, respectively, which in fact dominate the measured spectra.[28−34] A similar enhancement is expected for $[P^{met}]^{\bullet}$ so that the strongest bands in the high-frequency region at 1511 and 1590 cm^{-1} (Figure 4) are readily assigned to the A′ modes ν_{7a} and ν_{8a}, respectively. It is interesting to note that the ν_{8a} frequency is significantly lower than that of the *p*-$CH_3O-PhO^{\bullet}$. This decrease may be associated with the electron density distribution in the phenoxyl ring which, due to the additional *tert*-butyl substituents, should be increased in $[P^{met}]^{\bullet}$ as compared to *p*-$CH_3O-PhO^{\bullet}$ so that it may approach that of a phenolate. In fact, the ν_{8a} frequency of phenolate (1585 cm^{-1}) is close to that of $[P^{met}]^{\bullet}$.[44] Further assignments are given in Table 2 and in the Supporting Information.

Vibrational Assignments of Radical Complexes. Electrochemical oxidation of phenolato metal complexes containing the macrocyclic ligands L^{met} and L^{but} (Figure 1) leads to products which exhibit a strong absorption band at ca. 410 nm characteristic of phenoxyl radicals.[10,12−14,30] Evidently, coordination to the metal ion does not significantly affect the electronic transition. Hence, excitation in resonance with this transition should exclusively display the vibrational bands originating from the phenoxyl radical arm of the macrocyclic ligand. In fact, the RR spectra of $[Sc(^3L^{met})]^{+\bullet}$, $[Ga(^3L^{met})]^{+\bullet}$, and $[Ga(^3L^{but})]^{+\bullet}$ (Figure 5) are dominated by two bands at ca. 1500 and 1600 cm^{-1} which are readily assigned to the modes ν_{7a} and ν_{8a}, respectively, in analogy to the (free) *p*-$CH_3O-PhO^{\bullet}$, *p*-$CH_3-PhO^{\bullet}$, and $[P^{met}]^{\bullet}$ radicals. However, compared to that of the latter species[30] and $[Ga(^3L^{but})]^{+\bullet}$, the intensity ratio of both modes in $[Sc(^3L^{met})]^{+\bullet}$ and $[Ga(^3L^{met})]^{+\bullet}$ is reversed and accompanied by a substantial upshift of the ν_{8a} mode. It should be noted that the weak peak at 1631 cm^{-1} of $[Ga(^3L^{but})]^{+\bullet}$ cannot be assigned to the ν_{8a} mode but most likely results from an overtone (e.g., $2\nu_1$) or a combination mode. The corresponding Sc complex $[Sc(^3L^{but})]^{+\bullet}$ reveals a similar RR spectrum (not shown here); however, due to the instability of the complex, only the strongest bands at 1601 (ν_{8a}) and 1514 cm^{-1} (ν_{7a}) were detected. For *p*-$CH_3-PhO^{\bullet}$, the C−O stretching of the methoxy substituent was calculated at 1303 cm^{-1}. The RR spectra of $[Ga(^3L^{met})]^{+\bullet}$ and $[Sc(^3L^{met})]^{+\bullet}$ (as well as in related species with different metals; see below) reveal two very weak bands below and above 1303 cm^{-1}, while for $[Ga(^3L^{but})]^{+\bullet}$ only the low-frequency component is present. Thus, the high-frequency component for $[Ga(^3L^{met})]^{+\bullet}$ and $[Sc(^3L^{met})]^{+\bullet}$ is attributed to the C_4-O_2 stretching while the low-frequency band may be due to the ν_4 mode. Further assignments suggested in analogy to the free radicals are given in Table 2 and in the Supporting Information.

Enhancement Mechanism. Like those of the free phenoxyl species, the electronic absorption spectra of the metal-coordinated radical complexes exhibit a fine structure of the 410-nm band with a shoulder at high energies which is attributed to the 0→1 vibronic transition.[30] We have measured the RR spectra of $[Ga(^3L^{met})]^{+\bullet}$ with excitation wavelengths between 413 and 440 nm which are in resonance with both the 0→0 and the 0→1 transitions (Figure 6). The RR intensities of the bands were determined relative to the Raman bands of the solvent ($CH_3CN/LiClO_4$) which served as internal standard. The enhancement patterns of the individual bands are not uniform, and representative examples are displayed in Figure 7. All the modes are predominantly enhanced in resonance with the 0→0 transition implying that the *A* term (Franck−Condon) enhancement mechanism dominates.[45] In most cases, the intensity is significantly lower when the excitation wavelength is close to the high-energy shoulder of the transition (e.g., ν_{6a} in Figure 7). On the other hand, the ν_{9b} mode (1012 cm^{-1}) exhibits an increasing intensity below 420 nm, which is evident from the

(44) Harada, I.; Takeuchi, H. In *Spectroscopy of Biological Systems*; Clark, R. J. H., Hester, R. E., Eds.; Wiley: New York, 1986; pp 113−175.

(45) Albrecht, A. C. *J. Chem. Phys.* **1961**, *34*, 1476−1484.

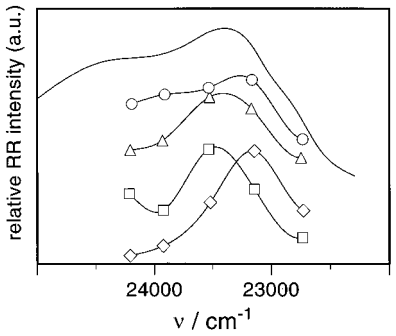

Figure 7. RR excitation profiles of various bands of $[Ga(^3L^{met})]^{+\bullet}$ compared with the absorption spectrum (solid line): ○, ν_{8a}; △, ν_{7a} (×4); □, ν_{9b} (×40); ◇, ν_{6a} (×20).

inspection of the spectra in Figure 6. Although the available data only provide a rather coarse excitation profile, it can be concluded that the ν_{9b} mode gains significant RR intensity in resonance with the 0→1 transition. This finding is consistent with the ca. 1000-cm^{-1} separation of the 0→1 and 0→0 transitions implying that this mode is also enhanced via the *B* term mechanism (vibronic coupling).[45,46] Also, the ν_{7a} and ν_{8a} modes appear to experience some *B* term enhancement, albeit much weaker than the ν_{9b} mode. It should be noted that in molecules of higher symmetry the selection rules are more rigid so that modes are enhanced either via the *A* or the *B* term.[46]

Parameters Controlling the Semiquinoid Structure of Phenoxyl Radicals. The bond length $C_{ortho}-C_{meta}$ is a measure for the semiquinoid character of the phenoxyl radicals. As shown in Figure 3, this structural parameter is correlated to the ν_{8a} mode frequency, which increases with decreasing bond length. Consequently, this mode can be regarded as a sensitive indicator for the semiquinoid structure, and in fact, the experimentally observed frequency for the *p*-benzosemiquinone radical (1613 cm^{-1})[28] is similar to that of the related *p*-$CH_3O-PhO^\bullet$ (1607 cm^{-1}). According to the data listed in Table 2, there is an increase of the ν_{8a} frequency and, hence, of the semiquinoid character, in the order $PhO^\bullet$ < *p*-$CH_3-PhO^\bullet$ < $[P^{met}]^\bullet$ < $[Ga(^3L^{but})]^{+\bullet}$ < *p*-$CH_3O-PhO^\bullet$ < $[Ga(^3L^{met})]^{+\bullet}$. This order can readily be understood in terms of two parameters controlling the semiquinoid structure: (i) An electron-donating substituent in *para* position is required which can withdraw spin density from the ring. In this respect, a methoxy group is more efficient than an alkyl group or a hydrogen as illustrated by the calculated spin densities in Table 1. However, additional alkyl substituents in the *ortho* positions such as in $[P^{met}]^\bullet$ appear to have an opposite effect, presumably since a further increase of electron density in the ring may afford a phenolate-like structure. (ii) The electron-accepting metal ion withdraws excess electron density from the ring by forming a coordinative $M-O_1$ bond with more or less π-bond character. Following these considerations, one would expect that also the ν_{7a} mode which includes the C_1-O_1 stretching coordinate parallels the changes of the ν_{8a} mode. However, such a relationship, if at all, only appears to hold for the free radicals. As will be shown in the following section, the mode ν_{7a} reflects the metal−phenoxyl interactions in a rather complex manner.

Metal Dependencies. Replacement of Ga or Sc by other metal ions does not change the overall vibrational band pattern of the RR spectra significantly. Thus, the vibrational assignments discussed for $[Ga(^3L^{met})]^{+\bullet}$ and $[Sc(^3L^{met})]^{+\bullet}$ can readily be extended to the other metal complexes (Table 2). For example, the RR spectrum of $[Fe(^3L^{met})]^{+\bullet}$, also obtained at

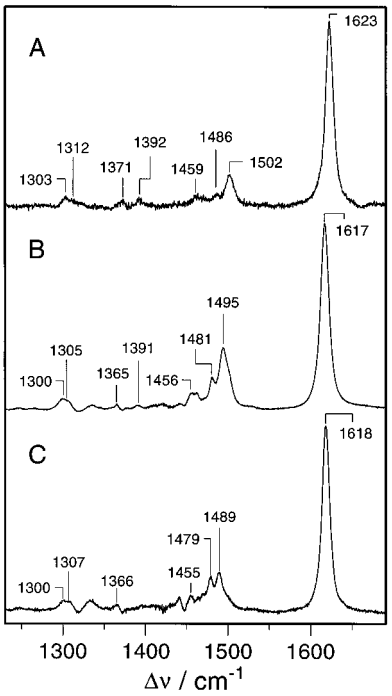

Figure 8. RR spectra of $[Fe(^3L^{met})]^{+\bullet}$ (λ_{exc} = 418 nm; A), $[Fe(^2L^{met})]^{+\bullet}$ (λ_{exc} = 427 nm; B), and $[Fe(^1L^{met})]^{+\bullet}$ (λ_{exc} = 427 nm; C) in the high-frequency region. The Raman bands of the solvent ($CH_3CN/LiClO_4$) are subtracted.

excitation in resonance with the $\pi \rightarrow \pi^*$ transition, is shown in Figure 8A; the RR spectra of the Zn and Cu complexes have been reported previously.[12,14] A careful comparison of the spectra shows that, notwithstanding the spectral similarities, some of the modes display distinct differences. In particular, we note substantial frequency shifts of the ν_{8a} and ν_{7a} modes within 15 and 9 cm^{-1}, respectively, for the various $[M(^3L^{met})]^{z+\bullet}$ (M = Ga, Sc, Fe; $z = 1$) and $[M(^3L^{met})H_n]^{(z+n)+\bullet}$ (M = Zn, Cu; $z = 0$) complexes with the latter having none ($n = 0$), one ($n = 1$), or two ($n = 2$) of the phenolates protonated (Table 2).

A detailed analysis of the spectra also reveals metal sensitivities for some weaker bands. For instance, mode ν_{19a} is found at ca. 1371−1374 cm^{-1} in the spectra of the Ga, Sc, and Fe complexes but at a substantially higher frequency in the spectra of the Zn complexes (1388 cm^{-1}). Furthermore, the C_4-O_2 stretching frequency increases with the ν_{8a} frequency.

The molecular origin of the metal sensitivity of the phenoxyl modes should be related to the electron-withdrawing capacity of the metal ion which, as discussed above, stabilizes the semiquinoid structure of the radical. This property of the metal ion is related to its capability to form π-bonds with the phenoxyl oxygen. It has been suggested[10] that this property can be expressed by an empirical parameter Δ (π-bonding parameter) which is the difference between the sum of the ionic radii of the metal and oxygen ion (according to Shannon[47]) and the experimentally determined M−O(phenolate) bond lengths of the parent complexes $[M(^3L^{met})]^0$ (taken from Adam et al.[10]). In Figure 9, this parameter Δ is plotted against the ν_{8a} frequency as well as the ($\nu_{8a} - \nu_{7a}$) frequency difference for the corresponding Fe, Ga, and Sc complexes. We also included the corresponding data for a Co(III) complex despite the different ligation pattern.[13] We note a decrease of the ν_{8a} frequency with the π-bonding parameter although the relationship is relatively crude. For instance, for the Ga and Fe radical

(46) Spiro, T. G. *Biochim. Biophys. Acta* **1975**, *416*, 169−189.

(47) Shannon, R. D. *Acta Crystallogr.* **1976**, *A32*, 751−767.

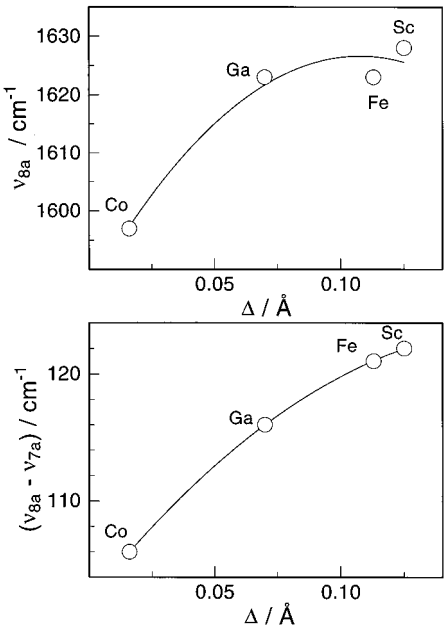

Figure 9. Plots of the π-bonding parameter Δ versus the ν_{8a} frequency (top) and the ($\nu_{8a} - \nu_{7a}$) frequency difference (bottom) for various $[M(^3L^{met})]^{+\bullet}$ complexes. Frequencies for the Sc, Ga, and Fe complexes were taken from Table 2, the frequencies for the Co complex from Sokolowski et al..[13] Further details are given in the text.

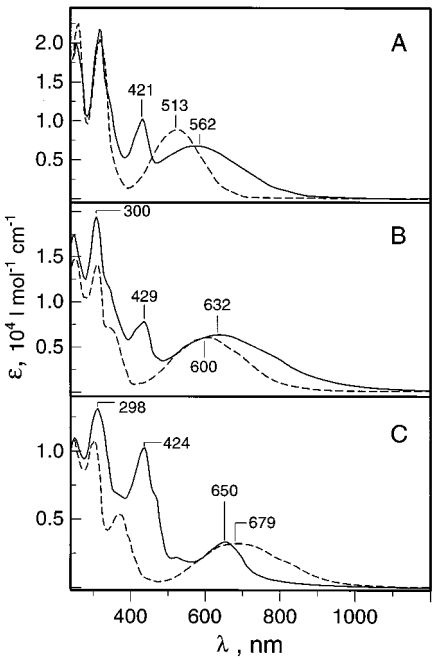

Figure 10. Absorption spectra of parent (dashed lines) and radical complexes (solid lines): A, $[Fe(^3L^{met})]^0$and $[Fe(^3L^{met})]^{+\bullet}$; B, $[Fe(^2L^{met})Cl]^0$ and $[Fe(^2L^{met})Cl]^{+\bullet}$; C, $[Fe(^2L^{met})Cl_2]^0$ and $[Fe(^2L^{met})Cl_2]^{+\bullet}$. All spectra were measured in $CH_3CN/LiClO_4$ solution.

complexes, the same ν_{8a} frequency is found whereas the π-bonding parameter is substantially larger for Fe. However, an unequivocal relationship is obtained when the frequency difference between both modes, ($\nu_{8a} - \nu_{7a}$), is plotted against Δ (Figure 9). The strongest π-bonding capacity and, hence, the largest frequency difference are found for Sc (122 cm^{-1}) due to its empty 3d orbitals whereas Co (106 cm^{-1}) shows just the opposite behavior in line with its $3d^6$ low-spin configuration. Note that for the uncoordinated radical, i.e., $[P^{met}]^{\bullet}$, this frequency difference is as low as 79 cm^{-1} (Table 2).

It appears that a strong π-bond character of the M−O_1 bond favors the semiquinoid structure. On the other hand, one would intuitively expect that a strengthening of this bond is paralleled by a weakening of the C_1−O_1 bond which eventually should exhibit the opposite effect on the electron density distribution in the phenoxyl ring (i.e., weakening of the C_{ortho}−C_{meta} bonds). This, however, is not observed, and also the ν_{7a} frequency, which may be taken as an indicator for the C_1−O_1 bond strength, does not vary systematically with the π-bonding parameter. These findings can be reconciled by taking into account that it is the excess electron density, introduced by the *o*-alkyl substituents (inductive effect), which is transferred to the M−O_1 bond and which otherwise would favor a phenolate-like structure. Thus, there appears to be a delicate balance between the effects of the electron-donating substituents (*p*-methoxy, *o*-alkyl) and the electron-accepting metal ion, or, correspondingly, between the strengthening of the C_{ortho}−C_{meta} and the weakening of the C_1−O_1 bonds. Consequently, it is not surprising that the absolute ν_{8a} and ν_{7a} frequencies are not good markers for the π-bonding parameter of the metal ion. On the other hand, the unequivocal correlation with the frequency difference ($\nu_{8a} - \nu_{7a}$) has to be regarded as an empirical one.

Summarizing the results on the free and coordinated phenoxyls discussed in this and in the preceding sections, we have two spectral markers which can be used to determine specific structural and electronic properties of the radical complexes. The frequency of the mode ν_{8a} can be taken as an unequivocal measure for the C_{ortho}−C_{meta} bond strength and, hence, the semiquinoid character of the phenoxyl ring, while the frequency difference ($\nu_{8a} - \nu_{7a}$) reflects the π-bond character of the M−O_1 coordinative bond.

Modification of the Coordination Pattern. So far we have implicitly assumed that the unpaired spin of the $[M(^3L^{met})]^{z+\bullet}$ and $[M(^3L^{met})H_n]^{(z+n)+\bullet}$ complexes is localized in one phenoxyl ring. This has in fact been demonstrated for Fe and Cu complexes as well as for $[Zn(^3L^{met})H_2]^{\bullet}$, while for $[Zn(^3L^{met})]^{2+\bullet}$ and the corresponding Ga and Sc species it was found that the spin is delocalized over all three aromatic rings on the EPR time scale.[10,11,13,14] Delocalization on the RR time scale, however, is not very likely, as it would imply interligand electron-transfer rate constants which are faster than 10^{12} s^{-1}. Moreover, a quantum chemical delocalization can be ruled out as well, since the RR spectra would differ significantly from those of the complexes with localized unpaired spin.

Thus, modification of the macrocyclic ligand by replacing one or two of the (nonoxidized) phenolates by more innocent ligands should provide information about nondynamic phenolate−phenoxyl ligand interactions. We have chosen the Fe complexes with the ligands $^2L^{met}$ and $^1L^{met}$ in which one and two phenolates are removed, respectively (Figure 1), and the vacant coordination sites are occupied by Cl^-. Radical complexes of these species, prepared by electrochemical oxidation, show the same characteristic ∼420-nm absorption band as the $[Fe(^3L^{met})]^{+\bullet}$ complex (Figure 10). The RR spectra of these radical complexes, excited in resonance with this transition, are compared with that of $[Fe(^3L^{met})]^{+\bullet}$ in Figure 8. Again, the overall vibrational band pattern reveals remarkable similarities, but with regard to the structure-sensitive spectral parameters, we note that the frequency difference ($\nu_{8a} - \nu_{7a}$) increases in the order $[Fe(^3L^{met})]^{+\bullet}$ (121 cm^{-1}) < $[Fe(^2L^{met})Cl]^{+\bullet}$ (122 cm^{-1}) < $[Fe(^1L^{met})Cl_2]^{+\bullet}$ (127 cm^{-1}), indicating an increase of the Fe−O_1 π-bond character. This tendency can readily be understood since the π-donating phenolates can effectively compete with the phenoxyl group for the half-filled t_{2g} orbitals of the Fe(III). Thus, the replacement of phenolate(s) by the less efficient π-electron

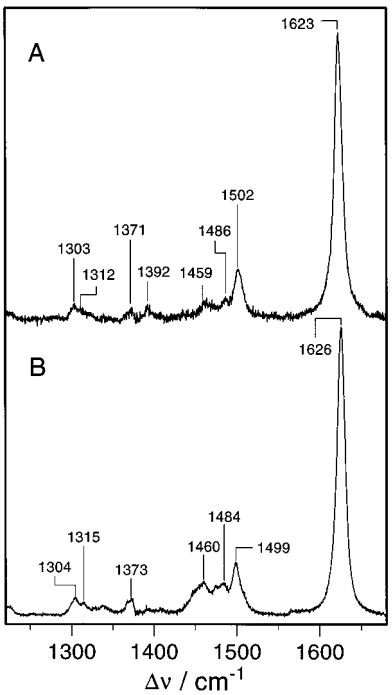

Figure 11. RR spectra of $[Fe(^3L^{met})]^{+\bullet}$ (λ_{exc} = 418 nm; A) and $[Fe(^3L^{met})]^{2+\bullet\bullet}$ (λ_{exc} = 430 nm; B) in the high-frequency region. The Raman bands of the solvent ($CH_3CN/LiClO_4$) are subtracted.

donor Cl^- should allow the phenoxyl group to form a stronger π-bond with the metal ion. On the other hand, this trend is not paralleled by an enhancement of the semiquinoid character, since the ν_{8a} frequency is even lowered from 1623 cm^{-1} to 1617 and 1618 cm^{-1} for $[Fe(^2L^{met})Cl]^{+\bullet}$ and $[Fe(^1L^{met})Cl_2]^{+\bullet}$, respectively. This finding suggests that, despite the increased Fe−O_1 π-bond character, reflected by an increase of the ($\nu_{8a} - \nu_{7a}$) difference, the electron density in the phenoxyl ring may be even slightly higher than in $[Fe(^3L^{met})]^{+\bullet}$ since the negative charge of the Cl^- ligands may be partially transferred via the Fe to the phenoxyl group. This effect should be much less pronounced in $[Fe(^3L^{met})]^{+\bullet}$ since the phenolate groups—although formally carrying the same charge—are capable of delocalizing the excess electron density within the ring itself. An analogous effect has been observed for the $^3L^{met}$ complexes of Zn and Cu after protonating one or two phenolates.[12,14] For $[M(^3L^{met})H_n]^{(z+n)+\bullet}$ the frequency difference ($\nu_{8a} - \nu_{7a}$) increases from 95 (n = 0) to 102 (n = 1) and 116 cm^{-1} (n = 2) in the Zn complexes and from 117 (n = 1) to 126 cm^{-1} (n = 2) in the Cu complexes, which can readily understood in terms of the weakened π-donating capability of phenols as compared to phenolates.

The Diradical Iron Complex. The parent Fe complex $[Fe(^3L^{met})]^0$ can be stepwise oxidized to yield the mono-, di-, and triradicals.[10] The absorption spectrum of the diradical complex is characterized by an increased oscillator strength of the ~420-nm absorption band implying that $\pi \rightarrow \pi^*$ transitions of both phenoxyl groups are largely independent from each other. The RR spectra of the mono- and the diradical, obtained in resonance with these transitions, are shown in Figure 11. The overall similarities between both spectra confirm the view that the two unpaired spins are localized in the individual phenoxyl rings. The small frequency differences for the marker modes ν_{8a} and ν_{7a} can, therefore, be interpreted under the same scheme as discussed for $[Fe(^3L^{met})]^{+\bullet}$, $[Fe(^2L^{met})Cl]^{+\bullet}$, and $[Fe(^1L^{met})Cl_2]^{+\bullet}$ (see above). The larger frequency difference ($\nu_{8a} - \nu_{7a}$) in the diradical complex (127 vs 121 cm^{-1}) is attributed to an increased Fe−O_1 π-bond character, implying that phenolates are stronger

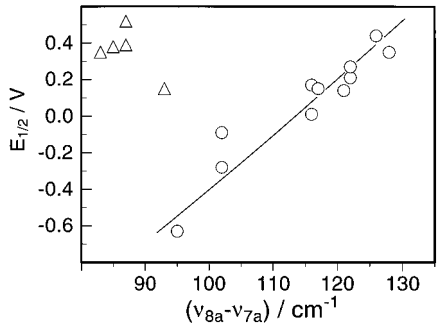

Figure 12. Correlation between the first redox potential $E_{1/2}$ (vs Fc^+/Fc) and the frequency difference ($\nu_{8a} - \nu_{7a}$) of the coordinated phenoxyls. The circles refer to the L^{met} and the triangles to the L^{but} radical complexes. The spectroscopic data were taken from Table 2 and from previous studies.[12−14]

π-donors than phenoxyl groups. In contrast to the cases of $[Fe(^2L^{met})Cl]^{+\bullet}$ and $[Fe(^1L^{met})Cl_2]^{+\bullet}$, however, the strengthening of the Fe−O_1 bond is accompanied by an increase of the semiquinoid character of the phenoxyl ring(s) since no excess electron density is transferred to the phenoxyl rings.

Correlations with the Redox Potential. As shown previously,[10] the oxidizability of the coordinated phenolate ligands depends on the strength of the metal−phenolate interactions, i.e., the π-bonding parameter Δ. Thus, the redox potential $E_{1/2}$ should be directly related to the frequency difference ($\nu_{8a} - \nu_{7a}$), which, in turn, has been shown to be proportional to Δ (see Figure 9). Indeed, Figure 12 displays a clear correlation between ($\nu_{8a} - \nu_{7a}$) and $E_{1/2}$ for all complexes carrying phenolates (1, 2, or 3) with a methoxy substituent in *para* position (circles). Whether such a correlation exists for the corresponding complexes with L^{but} ligands (open triangles in Figure 12) cannot be decided yet since the available body of experimental data is too small.

Selective Enhancement of the Phenolate Modes. In the reduced states, complexes of L^{met} or L^{but} containing a metal ion with a d^0 (Ga, Sc) or d^{10} (Zn) electron configuration do not exhibit electronic transitions in the near-UV or visible region so that RR spectra of these parent states could not be obtained. The situation is different for the Fe complexes as shown in the absorption spectrum in Figure 10. In the reduced form, $[Fe(^3L^{met})]^0$, we note a strong and broad absorption band centered around 510 nm which originates from a phenolate → Fe charge transfer (CT) transition. Upon oxidation to radical complexes, this maximum shifts to the red accompanied by a substantial broadening. Excitation of the RR spectra in resonance with this transition promises to selectively probe the phenolate modes both in the parent and in the radical complexes. Thus, it should be possible to assess electronic effects of phenoxyl radical formation on the remaining phenolate ligands.

Figure 13 shows the RR spectra of the parent, $[Fe(^3L^{met})]^0$, and radical, $[Fe(^3L^{met})]^{+\bullet}$, complexes obtained with excitation wavelengths in resonance with either the CT or the radical $\pi \rightarrow \pi^*$ transitions. The RR spectrum of $[Fe(^3L^{met})]^0$, excited in resonance with the CT band (Figure 13A), is dominated by two bands at 1475.4 and 1601.3 cm^{-1} which are not detectable in the RR spectra of the monocationic radical complex excited at 418 nm, which *a posteriori* confirms the conclusion that phenolate bands are not enhanced in resonance with the radical $\pi \rightarrow \pi^*$ transition. Conversely, the strongest phenoxyl modes ν_{8a} and ν_{7a} are very weak in the RR spectrum of $[Fe(^3L^{met})]^{+\bullet}$ excited in the CT band at 571 nm. The intensities of these bands are slightly higher compared to those of the phenolate modes when the excitation line is shifted toward the blue side

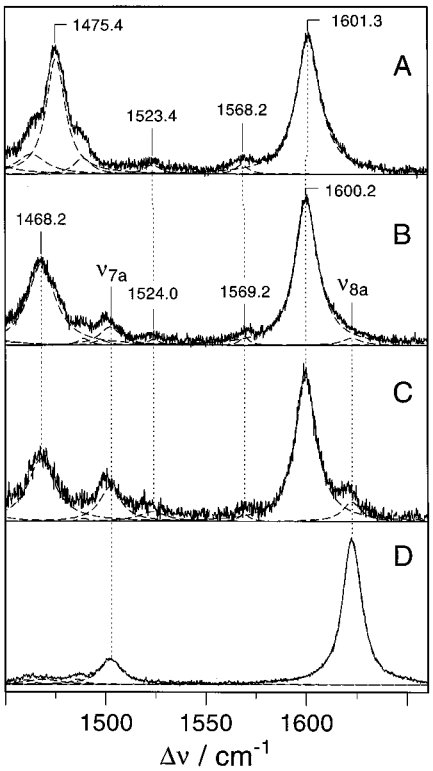

Figure 13. RR spectra of $[Fe(^3L^{met})]^0$ (λ_{exc} = 571 nm; A), $[Fe(^3L^{met})]^{+\bullet}$ (λ_{exc} = 571 nm; B), $[Fe(^3L^{met})]^{+\bullet}$ (λ_{exc} = 514 nm; C), and $[Fe(^3L^{met})]^{+\bullet}$ (λ_{exc} = 418 nm; D). The dashed lines represent fitted Lorentzian line shapes.

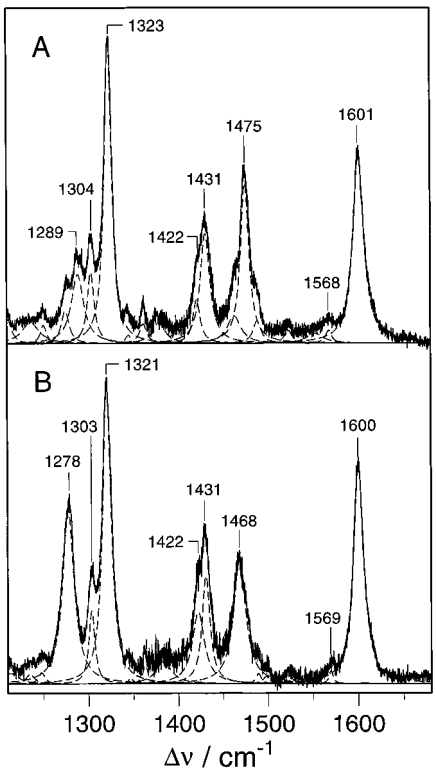

Figure 14. RR spectra of $[Fe(^3L^{met})]^0$ (A) and $[Fe(^3L^{met})]^{+\bullet}$ (B) in the high-frequency region excited at 571 nm. In panel B the contribution of $[Fe(^3L^{met})]^0$ and the RR bands of the phenoxyl ligand are subtracted as described in the text. The Raman bands of the solvent (CH_3CN/$LiClO_4$) are subtracted in both spectra. The dashed lines represent fitted Lorentzian line shapes.

of the CT band, i.e., at 514 nm. This implies that the significantly broadened absorption band in the spectrum of the radical complex includes also a contribution from a phenoxyl → Fe CT transition, presumably located at the high-energy side of the absorption band envelope, while the phenolate → Fe CT transitions are shifted to lower energies as compared to the parent state. This trend appears to be further enhanced in the diradical complex (Figure 10). Comparison of the spectra of $[Fe(^3L^{met})]^0$ and $[Fe(^3L^{met})]^{+\bullet}$, excited at 571 nm, indicates that radical formation affects the modes of the remaining phenolates. For instance, the 1601.3-cm^{-1} and, in particular, the 1475.4-cm^{-1} band are downshifted in $[Fe(^3L^{met})]^{+\bullet}$. Hence, it is desirable to obtain pure spectra of the coordinated phenolate of both $[Fe(^3L^{met})]^0$ and $[Fe(^3L^{met})]^{+\bullet}$. Thus, for the latter species the weak bands of the phenoxyl group (i.e., ν_{8a} and ν_{7a}) as well as residual contributions from the nonoxidized $[Fe(^3L^{met})]^0$ complex have to be subtracted on the basis of a component analysis of the spectra.[18] The RR spectra of $[Fe(^3L^{met})]^0$ and $[Fe(^3L^{met})]^{+\bullet}$ as well as of $[Fe(^3L^{but})]^0$ and $[Fe(^3L^{but})]^{+\bullet}$ which are obtained in this way are shown in Figures 14−17.

Vibrational Assignments for Phenolates. In general, the RR spectra of the coordinated phenolates display a significantly more complex band pattern than is observed for the phenoxyl radicals (cf. Figure 11), implying that upon resonance with the CT transition a larger number of modes gain considerable RR intensity. Moreover, for both the *tert*-butyl- and the methoxy-substituted phenolates, the RR spectra of the complexes reveal substantial changes of the frequencies and relative intensities between $[Fe(^3L^{met})]^0$ and $[Fe(^3L^{met})]^{+\bullet}$, indicating the phenoxyl formation has a distinct effect on the electronic and structural properties of the phenolates. Extracting this information from the spectra requires a safe vibrational assignment which, however, is not yet available for such asymmetrically substituted phenolates. Quantum chemical force field calculations of (phenolate) anions encounter the difficulty of an adequate description of the excess electron density at the periphery of the anion. Extended basis sets with Gaussian type orbitals (triple-ζ type with d- and p-polarization functions but without diffuse s and p functions) do not provide satisfactory results. Calculated frequencies of modes involving the C_1-O_1 stretching coordinate, in particular, of the mode ν_{7a}, were higher than the experimental values. Using the 9s5p/4s2p basis set augmented by polarization and diffuse s and p functions led to a notable improvement as demonstrated for PhO^- although there is still a significant deviation for mode ν_{7a}. This discrepancy is not surprising since the experimental data refer to PhO^- dissolved in alkaline solution[34,44] and solvation effects are likely to exert an important influence on the electron density distribution particularly of the oxygen, thereby affecting the corresponding force constants. Nevertheless, with the exception of this mode, even the unscaled calculated frequencies agree in a satisfactory manner with the observed bands for which assignments have been proposed on the basis of the spectra of isotopically modified phenolate derivatives.[34] These data are given in the Supporting Information.

Assignments for $[Fe(^3L^{met})]^0$ and $[Fe(^3L^{but})]^0$. Extending the assignments to the metal-coordinated phenolates is not as straightforward as in the case of the corresponding radical since the RR spectra display a much richer vibrational band pattern (Figures 14−17). This discrepancy may be related to the nature of the underlying electronic transition, i.e., a phenolate → Fe CT vs an intraligand $\pi \rightarrow \pi^*$ transition in the spectra of the radical.

There is no doubt that the band at 1601 cm^{-1} in the spectra of both $[Fe(^3L^{met})]^0$ and $[Fe(^3L^{but})]^0$ originates from mode ν_{8a}. Its frequency is the same for both complexes, which is in line

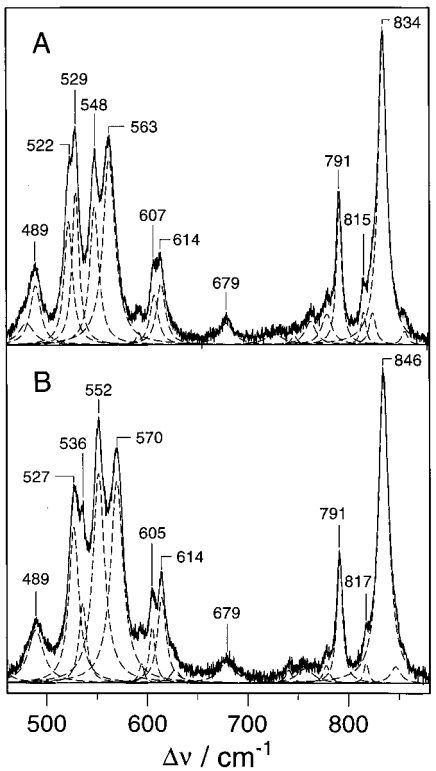

Figure 15. RR spectra of $[Fe(^3L^{met})]^0$ (A) and $[Fe(^3L^{met})]^{+\bullet}$ (B) in the low-frequency region excited at 571 nm. In panel B the contribution of $[Fe(^3L^{met})]^0$ and the RR bands of the phenoxyl ligand are subtracted as described in the text. The Raman bands of the solvent (CH_3CN/$LiClO_4$) are subtracted in both spectra. The dashed lines represent fitted Lorentzian line shapes.

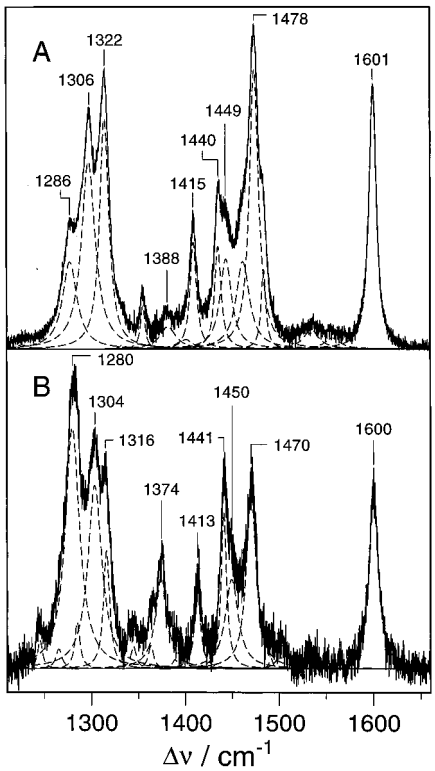

Figure 16. RR spectra of $[Fe(^3L^{but})]^0$ (A) and $[Fe(^3L^{but})]^{+\bullet}$ (B) in the high-frequency region excited at 514 nm. In panel B the contribution of $[Fe(^3L^{but})]^0$ and the RR bands of the phenoxyl ligand are subtracted as described in the text. The Raman bands of the solvent (CH_3CN/$LiClO_4$) are subtracted in both spectra. The dashed lines represent fitted Lorentzian line shapes.

with the calculations for the *p*-methyl- and *p*-methoxy-substituted phenolates. This is also true for the ν_{7a} mode which is assigned to the bands at 1289 and 1286 cm^{-1} of $[Fe(^3L^{met})]^0$ and $[Fe(^3L^{but})]^0$, respectively. In the low-frequency region (Figures 15A and 17A) the strong bands at 834 and 846 cm^{-1} are readily attributed to the ν_1 mode (ring breathing) of $[Fe(^3L^{met})]^0$ and $[Fe(^3L^{but})]^0$, respectively.

Phenoxyl−Phenolate Interactions in $[Fe(^3L^{met})]^{+\bullet}$ and $[Fe(^3L^{but})]^{+\bullet}$. Comparison of the RR spectra of the coordinated phenolates of the reduced state with those of the oxidized (radical) complexes reveals substantial differences in both the frequencies and the relative intensities. The frequency shifts are of particular interest since they reflect structural differences and changes of the electron density distribution in the ground state of two phenolates, brought about by the oxidation of the third phenolate. One of the largest frequency shifts is noted for ν_{7a} which downshifts by 9 and 6 cm^{-1} in $[Fe(^3L^{met})]^{+\bullet}$ and $[Fe(^3L^{but})]^{+\bullet}$, respectively, implying that the C_1-O_1 bonds are weakened. This can qualitatively be understood by assuming that there is a net transfer of electron density from the phenolates to the phenoxyl. Similarly large frequency shifts of ca. 7 cm^{-1} are observed for the bands at ca. 530 and 1475 cm^{-1} in the spectra of both the $^3L^{met}$- and $^3L^{but}$-derived complexes. Other frequency differences do not refer to the same modes of $[Fe(^3L^{met})]^{+\bullet}$ and $[Fe(^3L^{but})]^{+\bullet}$, implying that the phenoxyl radical alters the structures of the *p*-methoxy- and *p*-*tert*-butyl-substituted phenolates in a specific way. Characteristic examples are the bands at 1388 and 1322 cm^{-1} of $[Fe(^3L^{but})]^0$ and the bands at 834 and 563 cm^{-1} of $[Fe(^3L^{met})]^0$. Structural changes of a bystanding innocent ligand upon radical formation are also observed in Zn complexes where two coordinating phenolates were replaced by a bidentate 1,3-diphenyl-1,3-propanedionate (Ph_2acac^-).[14] The observed RR bands of the coordinated Ph_2acac^- exhibit comparably large frequency shifts (up to 7 cm^{-1}) upon oxidizing the coordinated phenolate to a phenoxyl.

Most of the frequency shifts observed in the spectra of $[Fe(^3L^{met})]^{+\bullet}$ and $[Fe(^3L^{but})]^{+\bullet}$ are accompanied by pronounced changes of the relative intensities. Thus the conclusion is justified that also in the CT-excited state the structure and electron density distribution of the phenolates are affected by the radical formation.

Implications for the Active Site in Galactose Oxidase. In the active site of GO, a copper(II) ion is coordinated by two tyrosinates, Tyr495 and the *ortho*-substituted Tyr272,[7] with the latter being oxidized to a tyrosyl in the active form of the enzyme. A tyrosyl radical is more closely related to a *p*-alkyl-substituted rather than to a *p*-methoxy-substituted phenoxyl, suggesting that metal complexes with L^{but} may be more realistic models for the biological system. Although for these complexes fewer experimental data are available as compared to the case of the L^{met}-derived species (Table 2), it is evident that, also for phenoxyl radicals with alkyl substituents in the *para* position, coordination to a metal ion increases the semiquinone character and, hence, the stability of the radical. This is reflected by the upshift of the ν_{8a} mode from 1577 cm^{-1} for *p*-$CH_3-PhO^\bullet$ (Table 2) to 1597 and 1601 cm^{-1} for $[Ga(^3L^{but})]^{+\bullet}$ and $[Sc(^3L^{but})]^{+\bullet}$, respectively, and to 1591 and 1593 cm^{-1} for $[Zn(^3L^{but})H_2]^{2+\bullet}$ and $[Cu(^3L^{but})H]^{+\bullet}$ (Table 2).[12,14] Thus, the ν_{8a} mode frequencies of the metal-coordinated species cover the range where also the corresponding mode of the copper-coordinated tyrosyl-272 has been identified, i.e., at 1595 cm^{-1}.[16] Hence, metal coordination of *p*-alkyl-substituted phenoxyl radicals causes an upshift of the ν_{8a} mode (10−20 cm^{-1}) similar to that for the

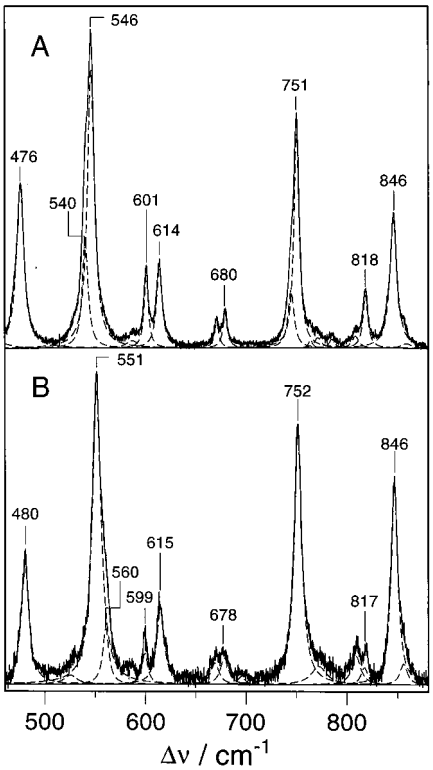

Figure 17. RR spectra of $[Fe(^3L^{but})]^0$ (A) and $[Fe(^3L^{but})]^{+\bullet}$ (B) in the low-frequency region excited at 571 nm. In panel B the contribution of $[Fe(^3L^{but})]^0$ and the RR bands of the phenoxyl ligand are subtracted as described in the text. The Raman bands of the solvent (CH_3CN/$LiClO_4$) are subtracted in both spectra. The dashed lines represent fitted Lorentzian line shapes.

corresponding L^{met}-derived complexes (cf. Table 2), implying that, in this respect, both types of radical complexes mimic the semiquinoid structure of the tyrosyl radical in GO.

On the other hand, the ($\nu_{8a} - \nu_{7a}$) frequency difference, a spectral marker which for $[M(^3L^{met})]^{+\bullet}$ species has been shown to be correlated with the π-bonding capability of the metal, is much larger for the copper-coordinated tyrosyl of GO (108 cm^{-1})[16] than for the metal-coordinated L^{but} radical complexes (83−93 cm^{-1}; see Table 2 and refs 12 and 14). This is also true for the analogous Cu radical complexes studied by Halfen et al.[27b] although an accurate determination of the band positions is difficult due to the unfavorable resonance conditions in that work. On the other hand, the frequency difference in GO is similar to those of $[M(^3L^{met})]^{+\bullet}$ complexes (>100 cm^{-1}; Table 2). In part, this relatively large frequency difference of the biological metal complex compared to the L^{but}-derived model complexes may be related to the fact that there are only two ligands competing for O→M π-bonding interactions in GO instead of three in $[M(^3L^{but})]^{+\bullet}$. Indeed, we have shown in this work ($[Fe(^3L^{met})]^{+\bullet}$, $[Fe(^2L^{met})Cl]^{+\bullet}$, $[Fe(^1L^{met})Cl_2]^{+\bullet}$) and in previous studies ($[Zn(^3L^{met})]^{\bullet}$, $[Zn(^3L^{met})H]^{+\bullet}$, $[Zn(^3L^{met})H_2]^{2+\bullet}$, and $[Cu(^3L^{met})H]^{+\bullet}$, $[Cu(^3L^{met})H_2]^{2+\bullet}$)[12,14] that the replacement of π-electron-donating phenolates by less efficient π-electron donors leads to a substantial increase of the ($\nu_{8a} - \nu_{7a}$) frequency difference of the remaining phenoxyl.

In addition, it may be that the *o*-thioether substituent of Tyr272, i.e., the covalent cross-linkage with Cys228, plays a role similar to that of the methoxy substituent in the L^{met}-derived radicals by donating electron density into the ring. This, however, implies that tyrosyl-272 assumes an *o*-semiquinoid structure as compared to the *p*-semiquinoid structures of the L^{met} model complexes.[48] In fact, the crystal structure of the inactive form of GO suggests a partial-double-bond character of the C_2-S_{cys} linkage in Tyr272.[7] Hence, the structural and functional role of the Cys substitution of Tyr272 may be the electronic stabilization of the radical in a manner analogous to that for the L^{met}-derived radical complexes. In fact, it was found recently[49] that the enzyme with an unsubstituted Tyr272 exhibits a substantially lower enzymatic activity and lower stability of the Cu(II) tyrosyl radical complex.

Conclusions

The RR spectroscopic analysis of $[M(^3L^{met})]^{z+\bullet}$ and $[M(^3L^{but})]^{z+\bullet}$ complexes essentially contributes to a better understanding of those parameters which control the spectroscopic features of coordinated phenoxyl radicals contrasting those of uncoordinated species. In particular, two sensitive spectral markers (frequency of ν_{8a} and the frequency difference $\nu_{8a} - \nu_{7a}$) have been identified which allow an unambiguous distinction between coordinated and uncoordinated phenoxyl radicals. These markers can also be monitored in redox enzymes involving tyrosyl radicals and, hence, promise to be particularly useful for elucidating structure−function relationships. The markers are related to the semiquinoid character of the phenoxyl structure (ν_{8a}) and its electronic stabilization by the covalently O-bound metal ion ($\nu_{8a} - \nu_{7a}$). Both parameters appear to balance the electron density distribution in the phenoxyl ring in a delicate manner.

Acknowledgment. P. H. gratefully acknowledges a Heisenberg fellowship from the Deutsche Forschungsgemeinschaft. We thank Professor W. B. Tolman (University of Minnesota) for making available his results[27b] prior to publication. Financial support by the Fonds der Chemischen Industrie is also gratefully acknowledged.

Supporting Information Available: Text and tables giving vibrational assignments for free phenoxyl radicals and coordinated radical complexes, including calculated and experimental normal-mode frequencies, and a table listing vibrational assignments for phenolate and coordinated phenolate complexes (10 pages). See any current masthead page for ordering and Web access instructions.

JA972269X

(48) For an *o*-semiquinoid structure, the highest-frequency ring mode ν_{8a} should predominantly include the stretching coordinates of the C_3-C_4 bond (adjacent to the *ortho* substituent at the C_2 atom) and the $C_{2'}-C_{3'}$ bond, which both are expected to exhibit the strongest π-bond character.

(49) Baron, A. J.; Stevens, C.; Wilmot, C.; Seneviratne, K. D.; Blakeley, V.; Dooley, D. M.; Phillips, S. E. V.; Knowles, P. F.; McPherson, M. J. *J. Biol. Chem.* **1994**, *269*, 25095−25105.